

# Mohammad I. Tradat

Department of Mechanical Engineering, ES2 Center, Binghamton University-SUNY, Binghamton, NY 13902 e-mail: mtradat1@binghamton.edu

# Yaman "Mohammad Ali" Manaserh

Department of Mechanical Engineering, ES2 Center, Binghamton University-SUNY, Binghamton, NY 13902

# **Ahmad Gharaibeh**

Department of Mechanical Engineering, ES2 Center, Binghamton University-SUNY, Binghamton, NY 13902

# Bahgat G. Sammakia

Department of Mechanical Engineering, ES2 Center, Binghamton University-SUNY, Binghamton, NY 13902

# Dave Hall

Department of Computer Science, ES2 Center, Binghamton University-SUNY, Binghamton, NY 13902

# Kourosh Nemati

Future Facilities, London SE1 7HX, UK; Future Facilities, New York, NY 10001

# Mark Seymour

Future Facilities, London SE1 7HX, UK; Future Facilities, New York, NY 10001

# Experimental and Numerical Analysis of Data Center Pressure and Flow Fields Induced by Backward and Forward CRAH Technology

An increasingly common power saving practice in data center thermal management is to swap out air cooling unit blower fans with electronically commutated plug fans, Although, both are centrifugal blowers. The blade design changes: forward versus backward curved with peak static efficiencies of 60% and 75%, respectively, which results in operation power savings. The side effects of which are not fully understood. Therefore, it has become necessary to develop an overall understanding of backward curved blowers and compare the resulting flow, pressure, and temperature fields with forwarding curved ones in which the induced fields are characterized, compared, and visualized in a reference data center which may aid data center planning and operation when making the decisions of which computer room air handler (CRAH) technology to be used. In this study, experimental and numerical characterization of backward curved blowers is introduced. Then, a physics-based computational fluid dynamics model is built using the 6SIGMAROOM tool to predict/simulate the measured fields. Five different scenarios were applied at the room level for the experimental characterization of the cooling units and another two scenarios were applied for comparison and illustration of the interaction between different CRAH technologies. Four scenarios were used to characterize a CRAH with backward curved blowers, during which a CRAH with forwarding curved was powered off. An alternate arrangement was examined to quantify the effect of possible flow constraints on the backward curved blower's performance. Then parametric and sensitivity of the baseline modeling are investigated and considered. Different operating conditions are applied at the room level for experimental characterization, comparison, and illustration of the interaction between different CRAH technologies. The measured data is plotted and compared with the computational fluid dynamics (CFD) model assessment to visualize the fields of interest. The results show that the fields are highly dependent on CRAH technology. The tile to CRAH airflow ratios for the flow constraints of scenarios 1, 2, 3, and 4 are 85.5%, 83.9%, 61%, and 59%, respectively. The corresponding leakage ratios are 14.5%, 16%, 38.9%, and 41%, respectively. Furthermore, the validated CFD model was used to investigate and compare the airflow pattern and plenum pressure distribution. Lastly, it is notable that a potential side effect of backward curved technology is the creation of an airflow dead zone. [DOI: 10.1115/1.4053890]

Keywords: data centers, EC plug fan, computational fluid dynamics, airflow distribution

### 1 Introduction

The amount of energy consumed by data center (DC) cooling is rapidly increasing and becoming a major concern for DC operators and managers due to increasing demand for DC services such as artificial intelligence, image processing, machine learning, and internet usage. Current trends seek to maximize data center utilization, reduce the energy consumed by information technology (IT) equipment and cooling infrastructure, and utilize cooling systems more efficiently. To that end, practical measurement tools and predictive models are needed to accurately capture the temperature, pressure, and flow fields of cooling and heating sources. A few examples of approaches that are often considered for reducing cooling energy consumption are direct and indirect evaporative cooling, wet-bulb economizer systems, data center best

Contributed by the Electronic and Photonic Packaging Division of ASME for publication in the JOURNAL OF ELECTRONIC PACKAGING. Manuscript received October 12, 2021; final manuscript received February 12, 2022; published online March 8, 2022. Assoc. Editor: Ronald Warzoha.

practices, and the implementation of more efficient cooling units such as electronically commutated (EC) plug fans [1–3].

In the literature, Hannman et al. [4] proposed an empirical-based measurement method to investigate the energy efficiency of best practices. In a different study, Radmehr et al. [5] used an averaged face velocity Pitot tube array to measure the volumetric airflow of the cooling unit and the perforated tiles in a raised-floor data center. The authors emphasized the integration of accurate facility transport measurements into data center infrastructure management tools based on computational fluid dynamics (CFD) for further predictions and management. The mismatch between the measured data and the CFD results was investigated by Iyengar et al. [6]. Their results showed that the maximum difference between the measurements and predictions was found at the air path between the exhaust of the server's rack and the intake side of the air cooling unit for a small data center cell.

Fluctuations in the tile airflow measurements in raised-floor data centers are induced by the turbulent residual component. Other factors that can cause variations in the margin of error include room size, perforated tile location, IT equipment

inventory, plenum geometry, and obstructions. The variations in the flow measurements can be  $\pm 10\%$  or more when impacted by the aforementioned factors. Therefore, significant flow measurement variations can make compact modeling and validation difficult. Nonetheless, compact modeling is widely used to predict and simulate the momentum transport through perforated tiles and pressure field variations. Large errors are expected when numerical and experimental errors are combined. Samadiani et al. [7] discussed floor grills modeling in their study. They added details to their six different models of the DC, including chiller pipelines and different tile open area ratios. They validated their numerical results with experimentally measured data. In a different study, a comparison between experimental and computational results was conducted by Abdelmaksoud et al. [8] to demonstrate the importance of considering the grill geometry details. Their results showed that tile modeling should account for opening patterns that affect the overall air-jet behavior. In another study by Garimella et al. [9] a summary of challenges and future trends for electronics thermal management was introduced as defined by experts in this field representing a wide range of industries. The authors showed that air cooling remains resilient as a data center cooling technique. Nada and Said [10] presented a CFD-based investigation of data center thermal management and airflow with different plenum depths, tiles openness, and rack power densities. They recommended 25-30% for the tile perforation and 60 cm as a suitable value for the plenum depth. Moazamigoodarzi et al. [11] presented CFD-based airflow and temperature field characteristic methodologies for three different architectures of DC cooling: room, row, and rack-based cooling. Their results showed a 29% reduction in the cooling power of row and rack cooling over the room. An additional reduction was accomplished by adding enclosures at the row and rack-level architectures. In another study, Lim and Chang [12] used CFD simulation to examine the effect of the servers' air outflow angles on their temperature fields. Their validated numerical results showed that an exhaust angle of 60 deg leads to the suppression of hot spots. The authors introduced two ventilation efficiency indices at a server level to pinpoint hot spots as well. Song et al. [13] proposed deflectors in cold aisle containment to improve the airflow distribution uniformity. Their experimentally validated numerical simulation proved the feasibility of applying such deflectors for airflow uniformity and hot spot elimination.

Computational fluid dynamics modeling was used to examine the effect of under-floor plenum obstructions on the thermal performance and tile flow delivery [14–16]. The researchers characterized the impact of underfloor blockages on DC performance and established guidelines in the form of a plenum color code. Moreover, they experimentally validated the guidelines in a different DC and presented a comparison of the numerical and experimental results. The results showed the severe impact of critically located blockages on reducing tile airflow by 19%. In a different study, Farazan Roknaldin [17] used the existing fan macromodel to develop a macromodel for a blower by introducing a systematic approach. The CFD results of this study were in alignment with the experimental results.

Stavreva and Serafimov [18] employed a CFD technique to investigate the velocity, temperature, and pressure fields of a dense data center. They studied and presented the impact of airflow distribution on energy efficiency. The results of their simulation found a potential method to improve the data center's energy efficiency, which was to adopt upgraded working conditions. Additionally, by using their CFD technique the authors discovered operational weak points within the dense DC.

Huang et al. [19] numerically studied three different levels of air-cooling using a CFD technique: underfloor, rack level, and row-level systems. Among the available cooling performance indices evaluated, the authors used the index of mixing, return temperature index,  $K_T$ ,  $\beta$ , and  $\eta_T$  to compare different cooling levels. The authors revealed that rack-level cooling showed the best performance with 0.0011 and 0.0082 values for the index of mixing and  $K_T$ , respectively. Moreover, Yann et al. [20] introduced

and analyzed a new concept of an in-rack-cold-aisle (IR-CA) system. The authors studied seven different rack intake crosssectional areas with an additional partition plane placed at the rack inlet. Their results revealed the optimal thermal distribution was obtained for the IR-CA case with the partition plane among the rest of the studied cases. In another study, using air to bypass the computer room air handler (CRAH) unit was proposed by Erden et al. [21]. The authors used tile fans to induce a fraction of room air into the pressurized underfloor plenum. Experimental verification of the flow network model and the thermodynamic model was introduced. An optimum bypass fraction was determined based on their analysis of the combined power consumption of the chiller and CRAH fans. Among the available turbulent models, Wibron et al. [22] examined a more advanced turbulence model's performance for data center CFD modeling. The authors considered the standard k- $\varepsilon$  model, the Reynolds stress model, and the detached eddy simulation using experimentally validated CFD. Both the Reynolds stress model and detached eddy simulation models had an advantage over the standard k- $\epsilon$  model, which failed to predict a low-velocity regime.

Wan et al. [23] surveyed and provided an overview of the current research that tends to improve the efficiency of air-cooling. Recently, Jin et al. [24] reviewed and summarized the aspects of airflow performance metrics and thermal optimization. The authors categorized the data center's thermal environment into three levels: room, rack, and server environments. The data center's airflow importance was emphasized. Based on their summary, the interactions of different factors such as location/CRACs model, plenum height, and perforated tile area openness percent need to be further investigated. In addition, Gong et al. [25] introduced a comprehensive review of the state of the art of thermal performance evaluation in data centers. They focused on metric characteristics and application levels (room, row, rack, and server levels). The authors discussed the advantages and limitations of major metrics and proposed an evaluation criterion for DC designers and operators to use the most appropriate indices for DC optimization. Huang et al. [26] investigated the effect of perforated tile arrangement on the airflow and temperature fields under nonuniform rack heat loads using numerical simulation. Under proper tile arrangement and openness

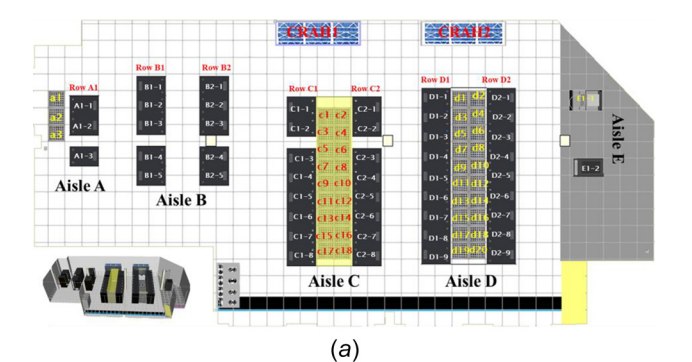
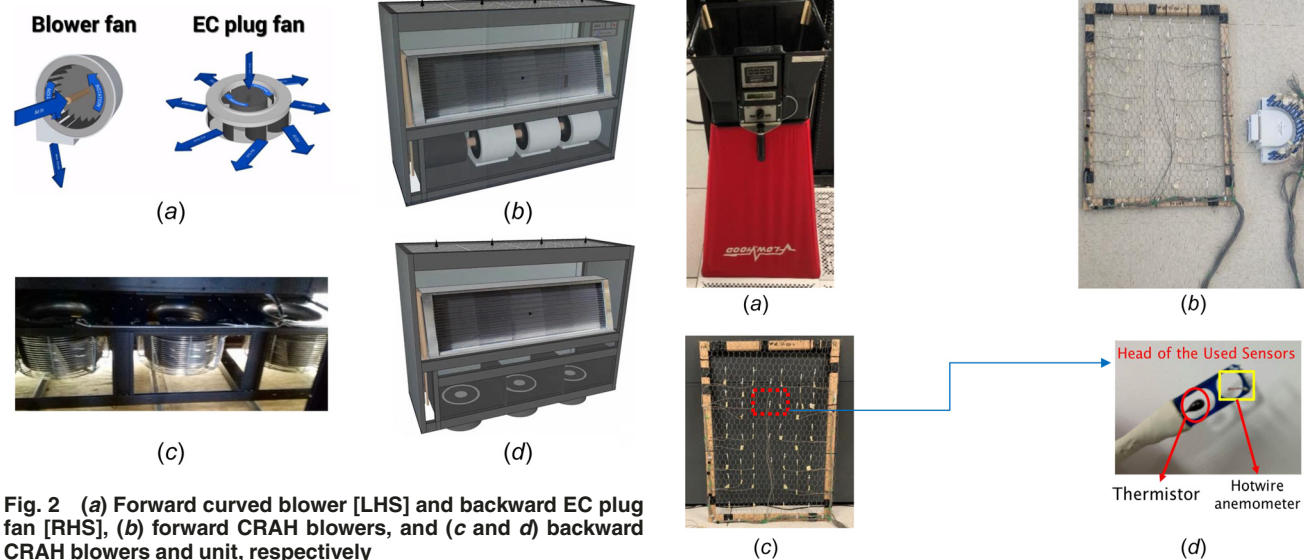




Fig. 1 ES2 DC lab: (a) racks and tiles matrix map view and (b) actual DC view



fan [RHS], (b) forward CRAH blowers, and (c and d) backward CRAH blowers and unit, respectively

ratio, they reported a 2.1 °C reduction in the maximum rack outlet temperature.

In this study, common data centers tools are used to measure the airflow rate, temperature fields above the tiles, and the pressure differential across the raised floor. A custom velocity/ temperature sensor grid was designed and built to measure the velocity and temperature fields at the intake of the cooling units for different operating conditions. The measured data is plotted, presented, and compared with a physics-based CFD model used later to visualize the fields of interest. The study aims to characterize and compare the flow, pressure, and temperature fields for different CRAH technologies using experimental measurements along with CFD visualizations. The results of this study can help to develop an understanding of different fields induced by different cooling units in a raised floor data center environment, to capture the hidden risk and key features of the produced momentum transfer by different blower technologies, and thus to guide

Fig. 3 Instrumentation: (a) flow hood, (b and c) the velocity/ temperature sensor grid, and (d) thermistor and hotwire anemometer sensor

(d)

capacity and installation planning of different units. The variations in airflow and pressure field measurements provide an important characteristic of backward curved blowers. The CFD visualization proves that these variations can be caused by the presence of a vortex, and in doing so, can also guide the installation of air driving technology to avoid or minimize the effect of vortices. To the best of the authors' knowledge, this is the first report of its kind that provides a detailed experimental and numerical analysis showing the effect and interaction of different CRAH technologies.

### 2 Experimental Characterization

2.1 Physical Domain Description. A plane view of the aircooled raised-floor data center laboratory, which is located at the

Table 1 Summary of cooling unit's specifications

Specification	CRAH 1	CRAH 2		
Overall dimensions (mm)	Both are identical with $[H \times W \times D]$ of $[1930 \times 3099 \times 899]$			
Blowers	Forward curved	Backward curved		
Static efficiency (%)	60	75		
Nominal flow rate (CFM)	16,500	17,300		
Nominal cooling capacity (Ton)	32	32		
Model	CW14DCVC	CW14DC1A		
Scoop availability	Available	Not Available		
Blower driving mechanism	All blowers are driven by variable speed motor	Each blower is driven by an independent EC motor		
Maximum power (kW)	10.23	9.5		

Table 2 Summary of tested scenarios and operating conditions

Scenario#	CRAH1 (blowers status)	CRAH2 (blowers status)	Aisle C doors (opened/closed)	Perforated tiles
1	OFF	ON	Opened	All tiles opened
2	OFF	ON	Closed	All tiles opened
3	OFF	ON	Opened	Blocked tiles in Aisles A and D
4	OFF	ON	Closed	Blocked tiles in Aisles A and D
5	ON	OFF	Opened	All tiles opened
6	ON at 50% variable frequency drive (VFD)	ON at 50% VFD	Opened	All tiles opened
7	ON at 100% VFD	ON at 100% VFD	Opened	All tiles opened

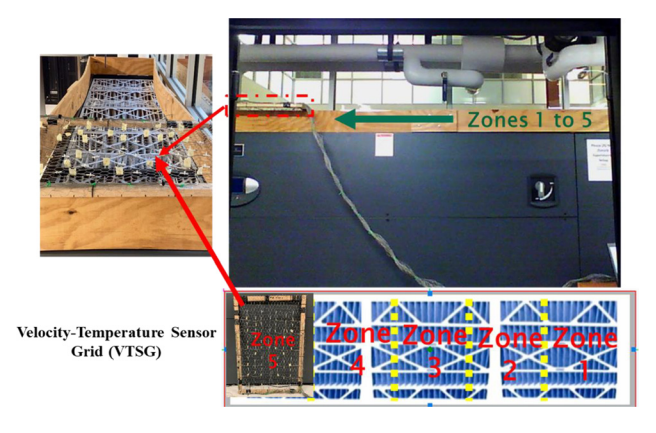


Fig. 4 Cooling units airflow rate measurements apparatus and method

State University of New York (SUNY) at Binghamton is illustrated in Fig. 1. There is a slab to slab height of 4.37 m (14.33 ft), which is broken down as follows: 0.91 m (3 ft) under-floor plenum depth and 3.45 m (11.3 ft) from the ceiling down to the raised floor. The room air is returned to two chilled-water cooling units. A traditional arrangement of hot aisle/cold aisle is used in the laboratory. The DC has an aisle pitch of 14 ft. The center to center distance between cold aisles varies between seven and nine

raised floor panels, each of which measures 2 ft × 2 ft. Furthermore, the perforated tiles in the cold aisles (A, C, and D) have a 22% open area. IT racks are placed in the white space of the real facility forming four cold aisles A, B, C, and D as follows: Aisle A is the network aisle that servers the other aisles and the data logging systems. Aisle B has no deployed IT equipment inside the IT racks. Aisle C is the main compute aisle where most of the IT load is concentrated. Finally, aisle D is mainly equipped with storage devices. Due to the low number of infrastructure blockages (chiller pipes), the underfloor plenum can be considered empty for the purposes of this study. A typical modern DC has modular air conditioning units and underfloor cool air distribution. The cooling cycle starts at the internally housed air handlers (i.e., CRAH1 and CRAH2). First, heat is extracted from the warm intake air thereby lowering its temperature, and the resulting cold air is supplied to the DC through the perforated tiles, after which it is forced across the IT equipment to carry away the produced heat.

2.2 Computer Room Air Handler Technology (Forward and Backward Curved Blowers). Backward curved blowers, which are driven by EC motors, are rapidly replacing traditional belt-driven forward curved blowers. The primary reasons are their increased operational efficiency, which is a result of avoiding the power losses associated with belt drives, and their reduced mechanical complexity, which increases the lifespan of the

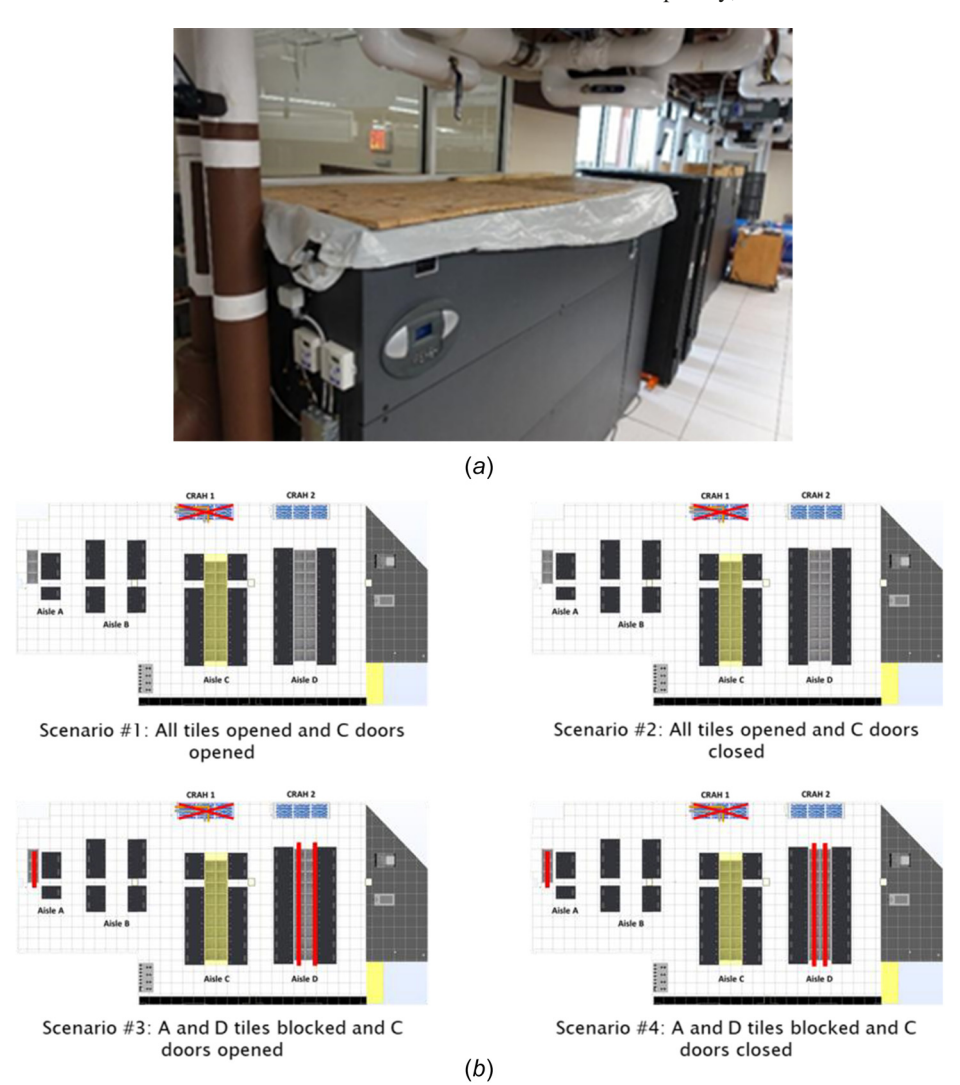


Fig. 5 (a) Covered CRAH1 intake and (b) experimental room level flow constraint scenarios for the EC plug fan cooling unit

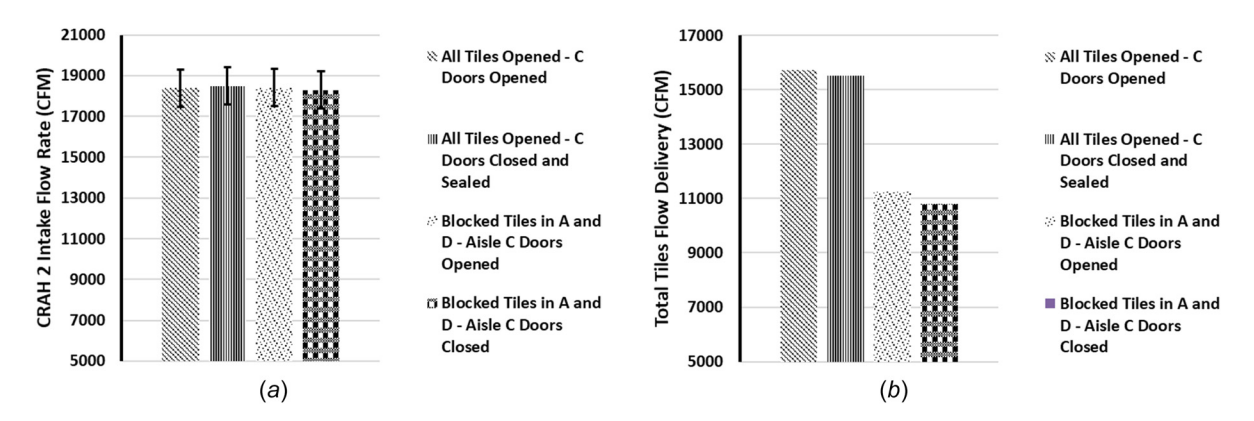


Fig. 6 Measured airflow rate: (a) at the intake of CRAH2 and (b) delivered through perforated tiles

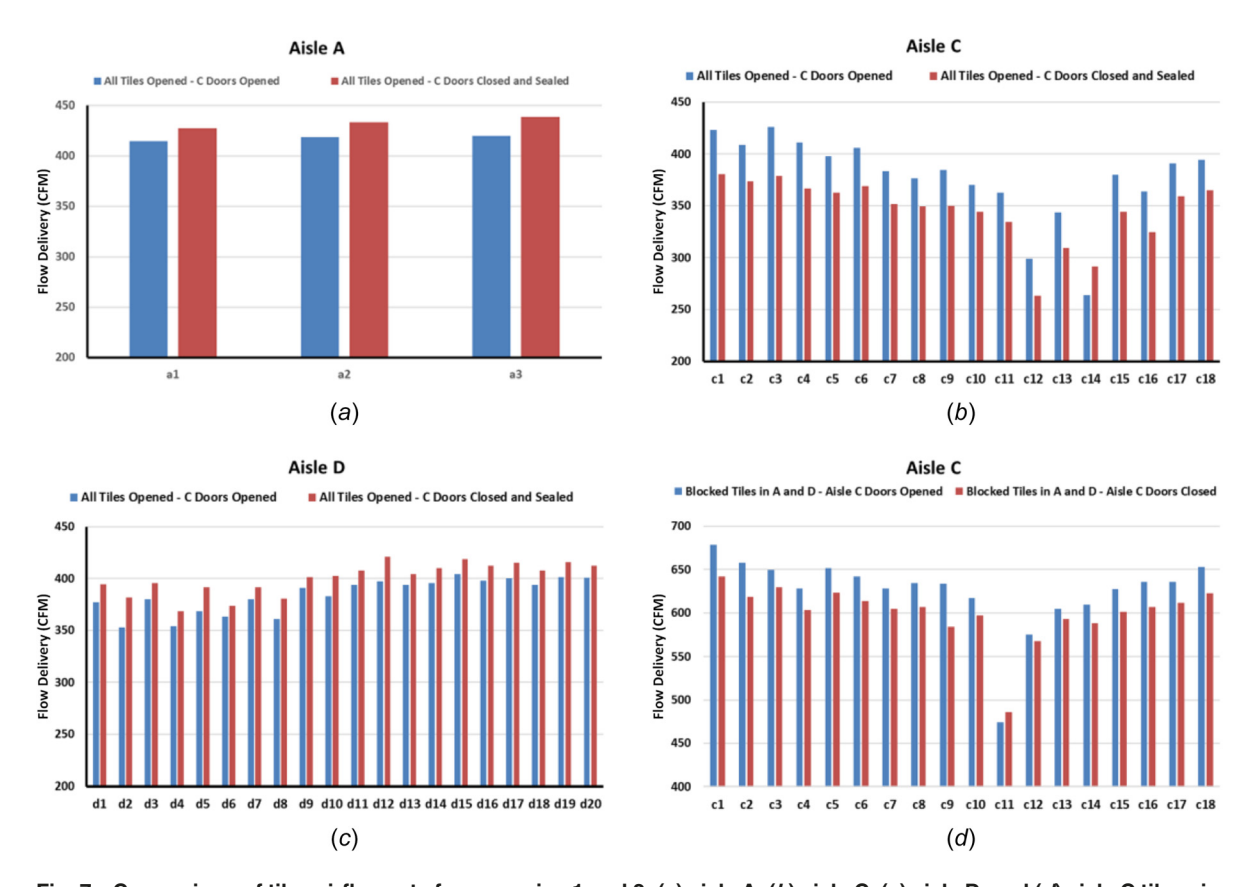


Fig. 7 Comparison of tiles airflow rate for scenarios 1 and 2: (a) aisle A, (b) aisle C, (c) aisle D, and (d) aisle C tiles airflow rate, scenarios 3 and 4

bearings. EC motors also provide a less complex method of controlling variable speed drive for the blower's wheel. Notably, backward curved blowers provide an airflow delivery pattern that is different from forwarding curved blowers: the change in blower design improves the peak static efficiency from 60% for forward curved blowers (per original equipment manufacturer (OEM)) to more than 75% for backward curved blowers.

Conventional forward curved blowers were previously studied [27]. The results of that study led to the installation of an EC driven backward curved blower unit (CRAH2) of identical dimensions and capacity. Both types are shown in Figs. 2(b) and 2(d). This entire unit has three EC plug fans and is also lowered into the plenum. It is attached to a separate chiller line and provides cool air directly to the plenum to support the deployment of additional IT. It is important to note that Liebert chilled water (CW) down-flow models equipped with EC driven backward curved blowers can be operated with the fans in the fully raised position

or lowered into the floor. The lower position provides these blowers with reduced air resistance and thus increased efficiency, but they also work well when not lowered. They are more efficient than forward curved blowers that have a bottom discharge with a mostly vertical downward velocity vector. Additionally, backward curved blowers gain more efficiency in the fully lowered position since air delivery is a combination of radial and tangential velocity. A summary of each cooling unit's specifications is provided in Table 1, as reported by the OEM technical manual.

Figure 2 illustrates a closer look at both blowers. In forward curved blowers, the air enters through the sides and is driven out in a downward direction by the in-place rotating blades. In backward curved blowers, the air enters through the top and is driven outward in all directions by the rotating blades.

**2.3 Experimental Setup.** An experimental characterization of the backward curved blower was conducted based on CRAH2

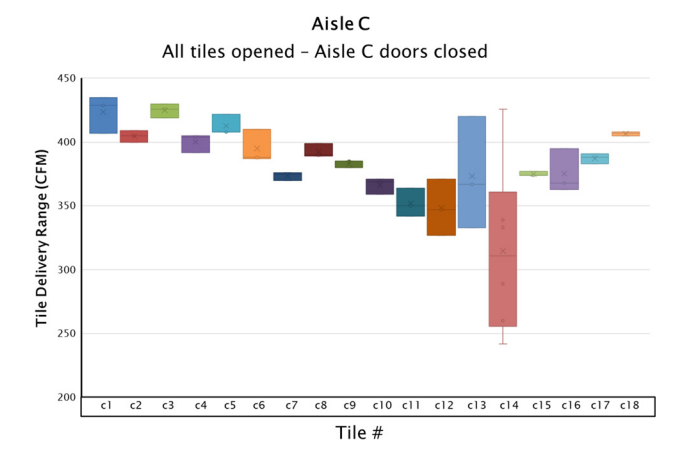


Fig. 8 Tile's flow measurement variations for scenario 2 and aisle  $\ensuremath{\text{\textbf{C}}}$ 

in the DC laboratory. The flow and pressure fields induced by CRAH1 and CRAH2 are compared. The tile airflow resulting from the interaction of both CRAH technologies is analyzed. Table 2 summarizes all of the studied scenarios and operating conditions. It is worth mentioning that scenarios 1-4 were used to characterize CRAH2, therefore, CRAH1 was powered off during these scenarios. Scenarios 6 and 7 were used to investigate the interaction of different CRAH technologies. An alternate arrangement was examined to quantify the effect of possible flow constraints on the backward curved blower's performance. Although Alissa et al. [27] previously presented experimental and analytical evaluations of CRAH1, the operating conditions in scenario 5 were conducted for comparison and model validation.

For all of the tested scenarios, most of the IT equipment in aisles C and D are powered off. Hence, heat dissipation in the facility can be broken as follows:

- 25 light emitting diode F8B lighting fixtures. Each has three bulbs with heat dissipation of 144 W, therefore, their share in the total heat dissipation can be approximated as 3.6 kW.
- 6–15 kW dissipated from a uninterruptible power supply unit (Galaxy EPS 6000, 300 KAV) depending on the battery's charge status and operation.
- 1.32 kW dissipated from a single-phase AC, 208-240 V, and 24 Amps PDUs.
- 42 kW dissipated from IT equipment that is kept running at idling computational load. These ITEs are kept running to not disturb other experiments and are considered during the data analysis and numerical model validation.

### 2.4 Tools and Measurement Methodology

2.4.1~ Flow Hood. As shown in Fig. 3, a flow hood (ADM-850 L) multimeter was used to report the airflow rate of the perforated tiles (locations shown in Fig. 1) for each test scenario with a measurement accuracy of  $\pm 3\%$  of reading and  $\pm 7$  CFM from 100 to 2000 CFM, as reported by the vendor technical manual. The device was equipped with an electronic micrometer to compensate for the additional flow impedance by the hood. The airflow balance provided backpressure airflow measurement, therefore, the error caused by the hood was eliminated. More information can be found in previous studies [28,29].

2.4.2 Velocity Temperature Sensor Grid. To measure the air velocity and temperature at the intake side of the cooling units, a custom velocity/temperature sensor grid was designed and built. As illustrated in Fig. 3, the sensor grid was installed on a wooden frame. A  $6 \times 6$  array of AccuSense TM UAS1200 sensors was installed on the grid mesh. These sensors are a hot wire anemometer and thermistor that measure the air velocity and temperature simultaneously. The sensor's measurement ranges are 0.15-5 m/s  $(30-400 \, \text{ft/min})$  and  $0-70\,^{\circ}\text{C}$   $(32-158\,^{\circ}\text{F})$  with an accuracy of  $\pm 5\%$  of the reading and  $\pm 1\,^{\circ}\text{C}$  for velocity and temperature, respectively. An ATM2400 data acquisition hub was used to

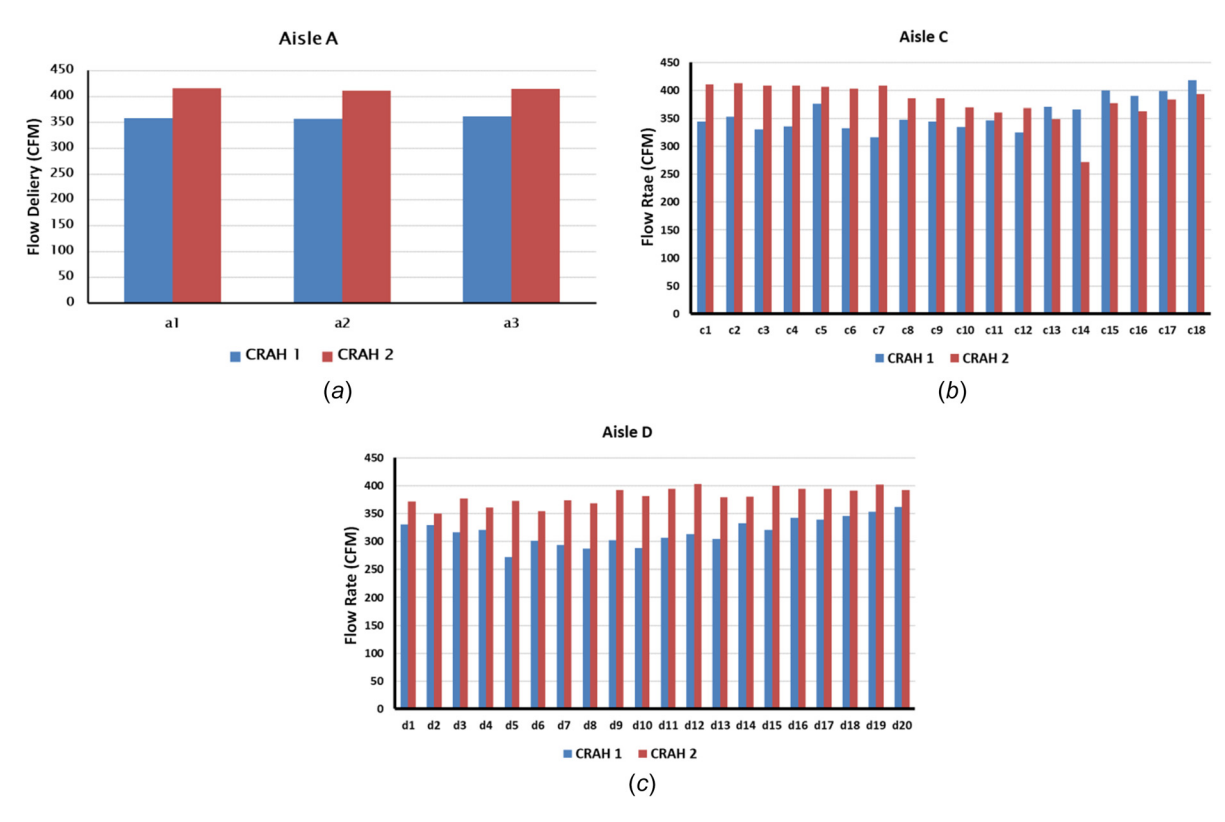


Fig. 9 Tile flow comparison for scenarios 1 and 5, aisles A, C, and D

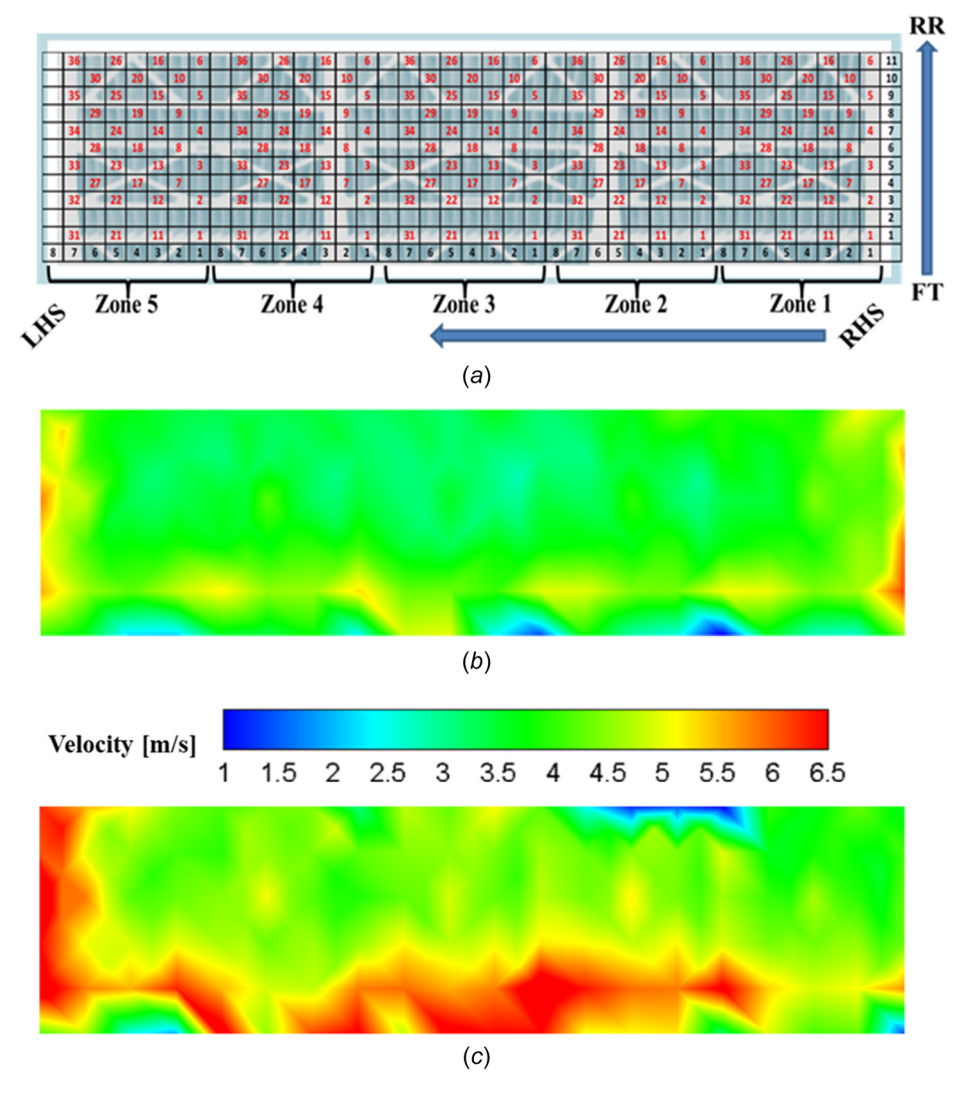


Fig. 10 (a) Sensors' locations at the return face of CRAH, (b) CRAH 1 velocity contours, and (c) CRAH 2 air velocity contours

attach all 36 sensors via a USB port. Simplicity, mobility, minimum disturbance of airflow or straightening effect, and remote collection of data features were factors considered in the design of this custom build.

2.4.3 Cooling Unit Intake Flow Measurement Methodology. The airflow of the cooling unit was measured using the velocity/ temperature sensor grid (VTSG). The intake side of the cooling unit was divided into five zones, as illustrated in Fig. 4. Each zone measured 24" wide. The VTSG depth was designed to be equal to CRAH unit depth. A traverse duct was used to restrict the normal component of return air velocity, as demonstrated in Fig. 4. This measurement methodology was used to report both air temperature and normal velocity components for the available CRAH technology (CRAH1 and CRAH2). Moreover, the reported velocities were used to estimate the nominal airflow capacity for each CRAH unit. On top of that, the reported data from the VTSG was used for the qualitative and quantitative analysis and illustration of the flow and temperature fields at the cooling unit's intake.

# 2.5 Results and Discussion

2.5.1 Characterizing CRAH2 Flow Field (Backward Curved Blower). To experimentally characterize CRAH2, four scenarios were considered, which are summarized in Table 2. In these

scenarios, CRAH1 was powered off and the intake side was covered to prevent backflow through the unit, as represented in Fig. 5(a). For scenarios 1 and 2, the doors of aisle C were opened and closed, respectively. This helped depict the effect of the flow resistance added by the cold aisle containment (CAC). Meanwhile, all of the perforated tiles were opened in both scenarios. For scenarios 3 and 4, the doors of aisle C were opened and closed, respectively. Meanwhile, the tiles of aisles A and D were blocked in both scenarios. CRAH2 intake flow was measured for all scenarios. Then, the total airflow rate was obtained by integrating all zones over the small square area  $(3 \times 3 \text{ in}^2)$  in the VTSG grid. Simultaneously, the airflow delivered to the aisle through the tiles was measured. The raised floor leakage through the seams and holes was estimated to be equal to the difference between the CRAH and tile airflows, and the measured raised floor gap was included in the CFD model. The model was thus able to report the leakage through the raised floor seems and pluming holes based on the specified gap size. According to Table 2 and for CRAH2 characterization the applied four-flow constraints are shown in Fig. 5(b).

Figure 6(a) presents the measured airflow rate at the return face of the CRAH unit. A similar reading was noted for scenarios 1–3, which was approximately 18,400 CFM. For scenario 4 the drop in the airflow rate was insignificant, approximately 211 CFM which counts for 1% of the total airflow. Based on this, it can be inferred

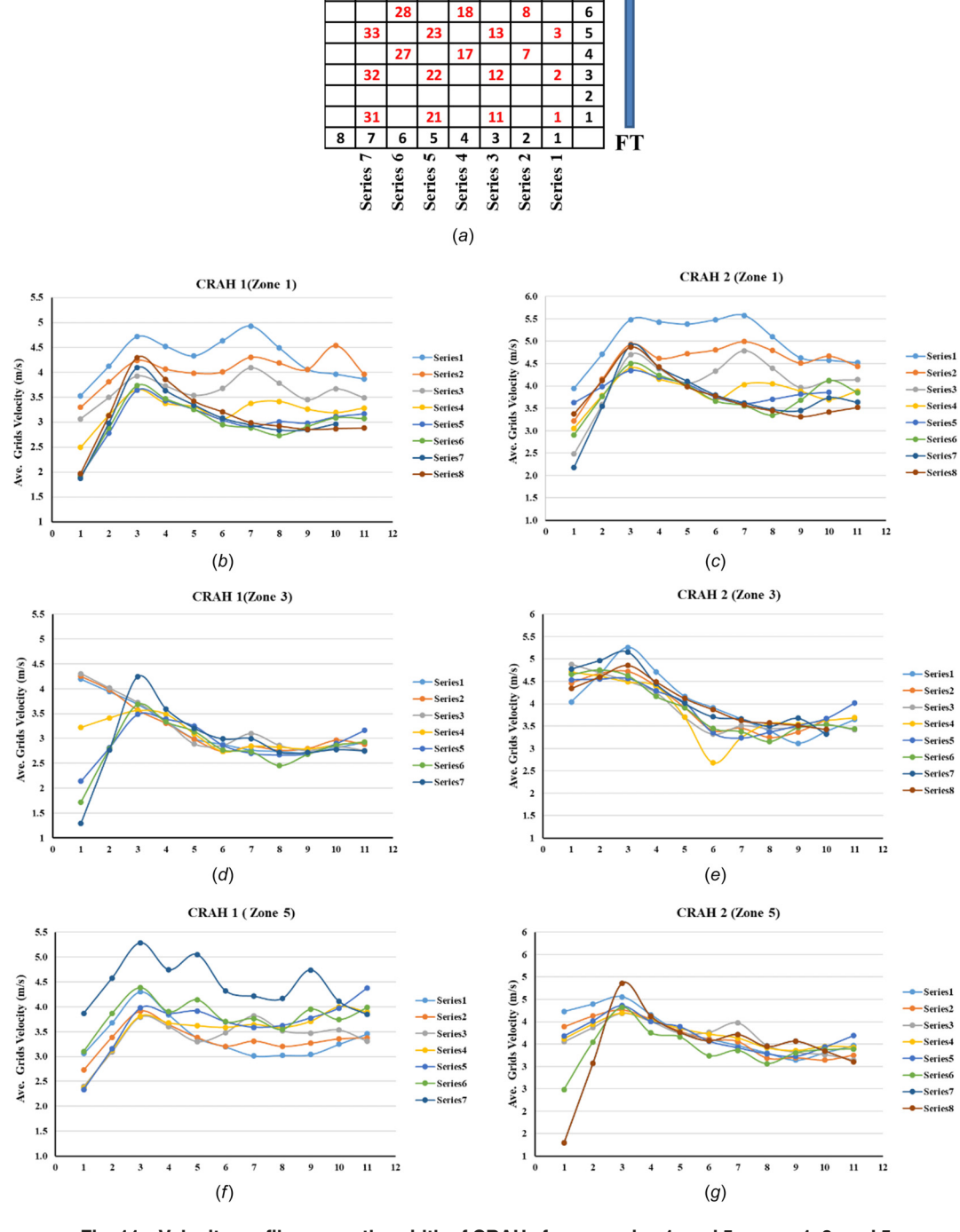


Fig. 11 Velocity profile across the width of CRAHs for scenarios 1, and 5, zones 1, 3, and 5  $\,$ 

that the containment doors had no effect on the cooling unit's airflow rate for scenarios 1 and 2. In scenario 3, when the tiles of aisles A and D were blocked while those of aisle C were opened, the floor leakage and voids reduced the effect of the flow constraint on the cooling unit's airflow rate. In scenario 4, the cooling unit airflow rate dropped insignificantly by 211 CFM due to the introduction of CAC compared to scenario 3. Next, Fig. 6(b) presents the total tile airflow rate. The tile airflow rate readings for scenarios 1 and 2 dropped by  $\sim$ 205 CFM due to the introduction of CAC. From scenarios 3 and 4, the tile's airflow rate dropped by approximately 437 CFM.

An important consideration for the measurement procedure in this study is the uncertainty of the hot wire sensors, which was about 5%. That amount of error corresponds to approximately 900 CFM. While the measurement procedure was useful for obtaining the cooling unit's airflow rate within a 5% margin of error, this uncertainty meant that the variation in room pressure could have been slightly overestimated.

A comparison of the individual tiles is demonstrated in Fig. 7. It can be inferred from this figure that containment in aisle C reduced the received flow and increased the airflow rates in the other aisles. The additional barrier to the air path in aisle C caused

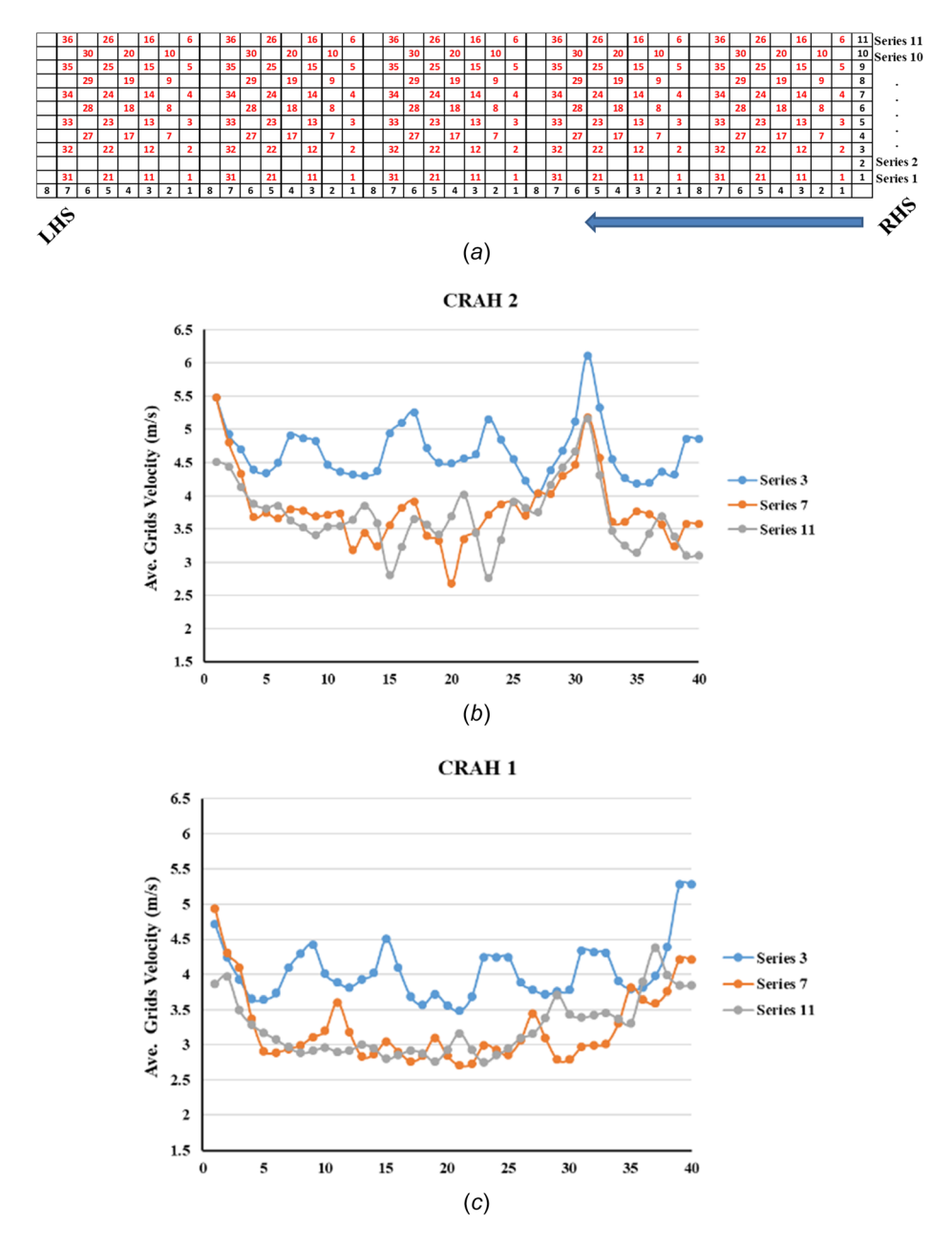


Fig. 12 Velocity profile across the length of CRAHs for scenarios 1 and 5, respectively

the total tile delivery to drop by 568 CFM. The reduced lower airflow was redirected to aisles A and D, while 205 CFM escaped through floor leakage paths. The amount of floor leakage was estimated to be 2658 and 2974 CFM for scenarios 1 and 2, respectively. These results indicate that floor leakage increased due to CAC. By restraining the flow to one aisle, in this case, aisle C, floor leakage increased significantly. For scenarios 3 and 4, the amount of leakage was estimated to be 7167 and 7495 CFM, respectively.

The tile to CRAH airflow ratios for the flow constraint in scenarios 1, 2, 3, and 4 were 85.5%, 83.9%, 61%, and 59%, respectively. The corresponding leakage ratios were 14.5%, 16%, 38.9%, and 41%, respectively. Furthermore, it can be noted from Figs. 7(b) and 7(d) that tiles c12, c14, and c11 always received a lower airflow rate than the other tiles.

Figure 8 illustrates the various plots of successive measurements over 2 min with a time-lapse of 15 s between successive measurements for the perforated tiles of aisle C in scenario 2. The variation in measurements was plotted. It can be noted that tiles

c14, c13, and c12 had higher variation. Those variations were caused by pressure wake under those tiles for which a vortex was suspected.

2.5.2 Backward and Forward Curved CRAH Technology Comparison of Tile's Airflow Delivery. To demonstrate a comparison of the airflow delivered through perforated tiles provided by a standalone cooling unit. Figure 9 sets individual perforated tiles side by side for scenarios 1 and 5, where only one cooling unit was on duty and the other one was powered off with the intake side covered, as shown earlier in Fig. 5(a). For both scenarios, all of the tiles were open and the CAC doors of aisle C were open. Thus, it can be assumed that the airflow resistance in each scenario is similar. It can be noted that the tile airflow delivery was always higher when CRAH2 was on duty, except for tiles c13, c14, c15, c16, c17, and c18. This was related to the airflow pattern out of the unit and to the spatial location of these tiles with respect to the cooling unit, where they were in close proximity to high

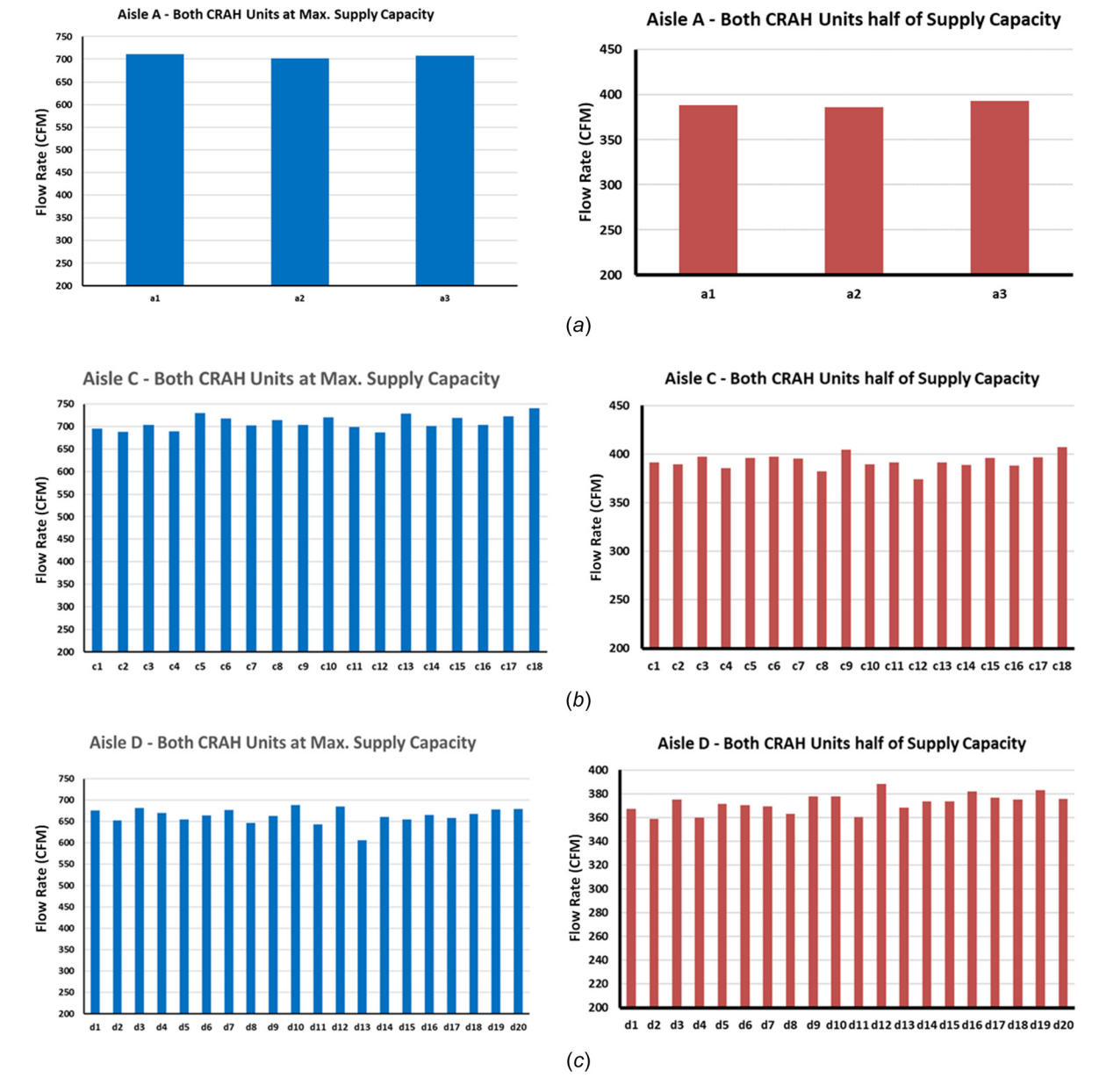


Fig. 13 Measured tiles airflow rate at different supply rates from CRAHs, maximum and half-nominal supply

static pressure near the wall. This is explained in more detail in the numerical section.

2.5.2.1 Velocity field and profile at the intake side of the cooling units. The air velocity contours and profiles were analyzed to investigate the effect of different CRAH technology on the air velocity across the width and length of the CRAH intake. In addition, part of these measurements is used later to validate the CFD model. Figure 10(a) demonstrates the velocity/temperature sensor distribution at the intake side of the cooling units. Figures 10(b)and 10(c) illustrate the air velocity contours of CRAH2 and CRAH1, respectively, for scenarios 1 and 5. It can be inferred from the figures that at CRAH1's intake the air velocity was lower and more uniform than at CRAH2's intake. Additionally, the figures show the high normal component of air velocity at the front and side edges of CRAH2, which could have been the result of many factors, such as the momentum transfer provided by different CRAH technology, sensor movement during the test, or the edge effect, which is higher for backward curved blowers. Furthermore, the zonal approach provided more flexibility when comparing the air velocity across the width of the cooling units, as

illustrated in Fig. 11(a). Each zone (refer to Fig. 10(a)) was divided into seven series. The air velocities measured across each series were plotted, as shown in Figs. 11(b)-11(g). The figure illustrates the edge effect, which is similar to the one previously discussed. This edge effect caused a decrease in the air velocity of zone 1, whilst the effect was reversed for zone 5 (Fig. 12).

2.5.2.2 Interaction of different CRAH technology. For insight into the interaction of the two different CRAH technologies, the flow, temperature, and pressure fields for scenarios 6 and 7 are compared. Figure 13 illustrates the tile's airflow rates in these scenarios, in which both CRAHs were on duty but with different supply capacities. The tiles airflow in aisles A and D exhibited similar behavior for both scenarios, whilst that of aisle C varied between each scenario. The results show that tile c8 reported a higher airflow rate compared to the adjacent tiles (c7 and c9) for scenario 7, whereas its airflow rate was lower for scenario 6. Other examples of this type of variation in aisle C between the scenarios can be found as well. Furthermore, the measured pressure differentials between the plenum and the room at different spatial locations for scenarios 1, 5, 6, and 7 are illustrated in Fig. 14. The

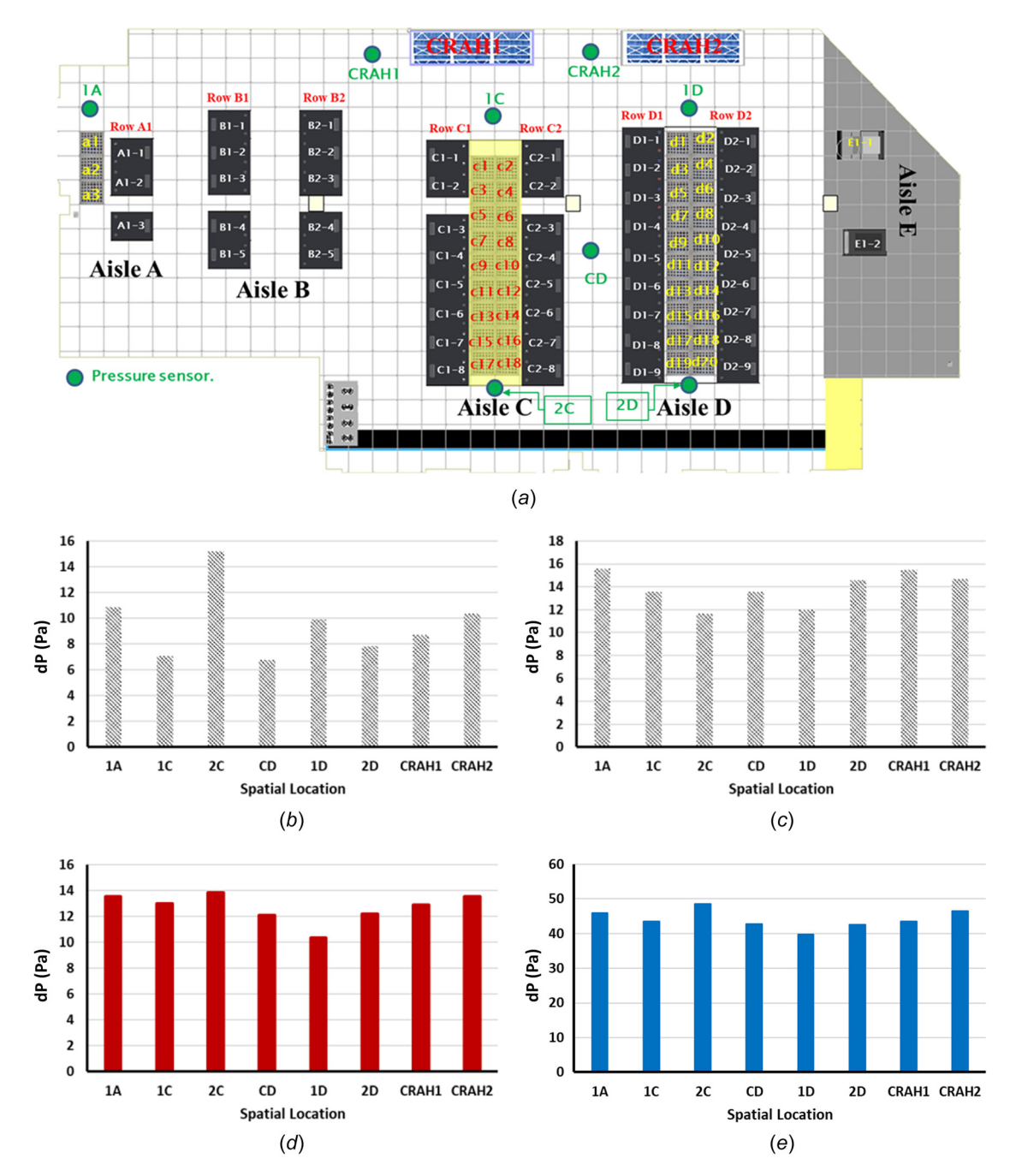


Fig. 14 (a) Spatial locations of pressure sensors that report differential pressure and (b-e) the pressure differential between the plenum and the room space for scenarios 5, 1, 6, and 7, respectively

results showed pressure maldistribution for all single CRAH scenarios with more uniformity noted when both CRAHs were on duty. Given the complex and turbulent nature of the airflow distribution in the underfloor plenum, the next part of the study will use a validated CFD model to visualize the flow, temperature, and pressure fields for the different CRAH technologies.

### 3 Numerical Modeling

Computational modeling is needed to reduce the time, cost, and risk associated with full-scale experiments. Therefore, the entire physical domain of the ES2 data center laboratory was replicated in a physics-based CFD model to visualize the flow, temperature, and pressure fields induced by the two different standalone CRAH technologies as well as the interaction of the two. In addition, the visualization illustrates the impact of different CRAH

technologies on the data center environment and the possible formation of hot spots at the intake side of IT equipment. A grid independence test was conducted by varying the mesh size and then a chosen number of grids was selected to quantify the confidence and predictive accuracy of the CFD model [30,31]. Adiabatic walls with no radiation heat transfer were assumed for the model. Air was assumed to be incompressible and have constant properties. Lastly, the wall roughness and body forces were considered negligible. Therefore, the classical Navier–Stokes, and energy governing equations were numerically solved Mass conservation

$$\nabla \cdot \underline{V} = 0 \tag{1}$$

<sup>&</sup>lt;sup>1</sup>https://www.futurefacilities.com/resources

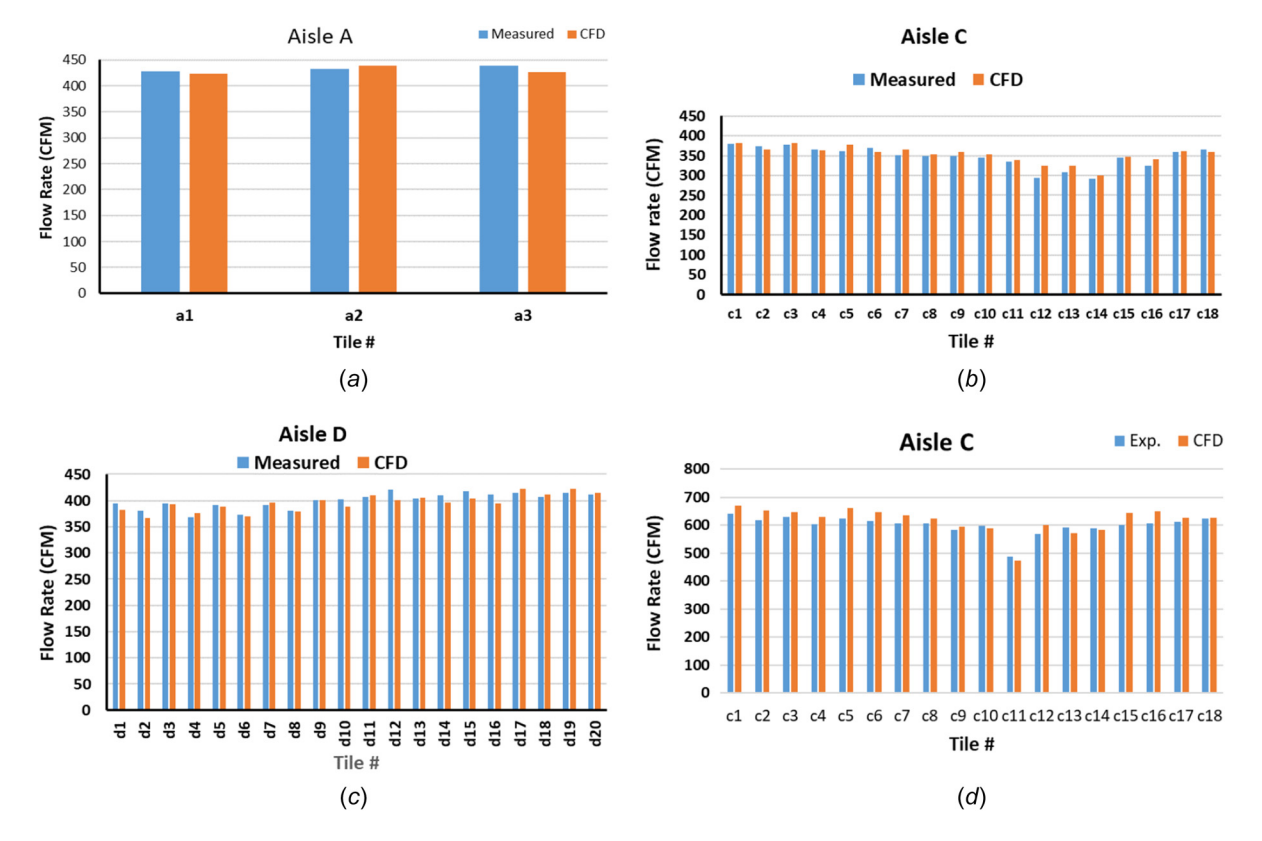


Fig. 15 Comparison between experiment and CFD tiles airflow rate results for (a–c) scenario 2 and (a) scenario 4

Momentum conservation

$$\rho \frac{D\underline{V}}{Dt} = -\nabla P + \mu \nabla^2 \underline{V} + \rho \underline{g}$$
 (2)

Energy conservation

$$\frac{D\underline{T}}{Dt} = \alpha \nabla^2 T + \frac{1}{\rho c_p} \phi \tag{3}$$

Given the turbulent nature of the flow in raised-floor data centers, the standard k– $\varepsilon$  model coupled with RANS equations was selected to simulate the flow fields. The selection of such a model was based on the available literature that confirmed the feasibility of employing it in data center simulations [32].

3.1 Model Validation. The quantified confidence and predictive accuracy of the ES2 data center CFD model have been developed and refined over several years under the supervision of a commercial software developer [29]. Furthermore, to ensure the model predictivity and accuracy for this study, the lumped fan model was adopted to model the fans due to its simplicity and the fact that it is computational cost effective. The geometry and specifications of the fans were imported from the OEM technical manuals and defined in the CFD model. The experimental operating conditions, summarized in Table 1 above, were imposed exactly in the CFD model. Thereafter, the modeling results were compared to the experimental ones. The comparison considered pressure, tile airflow rates, and temperature measurements at the intake side of the cooling unit, with an additional assessment of thermal IR images. It is worth mentioning that for all of the tested scenarios the supply air temperature was held constant at 68 °F (20 °C) and a constant thermal load was maintained.

Figure 15 presents a comparison of individual tile's average measured and CFD predicted airflow rates for scenarios 2 and 4.

The CFD model and the experiment agreed with a reasonable mismatch and a maximum absolute error of 8% in tiles' airflow rate. On the pressure side, Fig. 16 depicts the agreement between the average pressures reported by the pressure sensors at the preselected spatial coordinates in the DC room. Although the maximum calculated absolute error was 16.2%, the figures show good agreement between the CFD results and the experiment. As a final step of model validation, experimental quantitative and qualitative measures of air temperature at the intake side of the cooling unit were compared with the ones resulting from CFD simulation, as displayed in Figs. 17(a) and 17(b). In addition, Fig. 17(c) and 17(d) represent a thermal IR image for scenario 1. It can be inferred from the figure that there is good agreement between the predicted and actual thermal images as well as between the predicted and measured air temperatures. This validation of the physics-based CFD model highlights the importance of the digital twin for predicting the effect of any changes in the data center room.

3.2 Modeling Results and Discussion. Having established the level of agreement between the CFD model and experimental measurements, the pressure fields induced by the different CRAH technologies can be visualized and assessed. To that end, the pressure distribution across a horizontal plane in the plenum for all of the tested scenarios is illustrated in Fig. 18. Comparing the results for scenarios 1 and 2, it is apparent that the higher plenum pressure in scenario 2 indicates a more resistive airflow path due to the doors being closed. A similar pattern is evident between scenarios 3 and 4.

In addition, in the results for scenarios 1 and 5, the difference in the pressure fields induced by each CRAH technology is notable. The resulting fields were highly related to the direction of the CRAH outlet jets. For the forward curved blowers, the pressure increased as the distance from the CRAH increased vertically, with respect to the cooling unit.

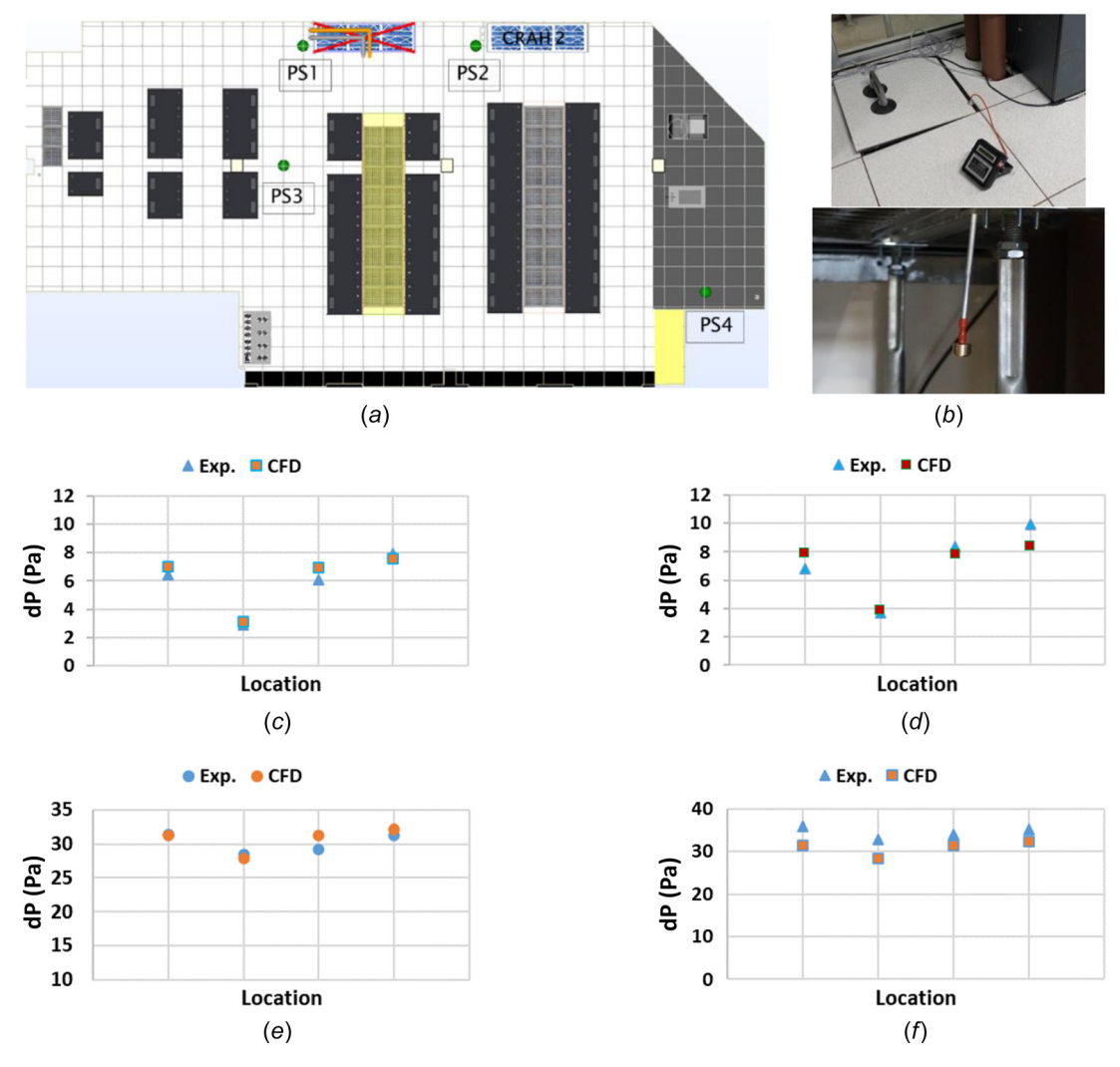


Fig. 16 (a) Locations of pressure differential measurements for CFD model validation, (b) pressure differential measurements (c-f) pressure differential experimental results versus CFD for scenarios 1, 2, 3, and 4, respectively

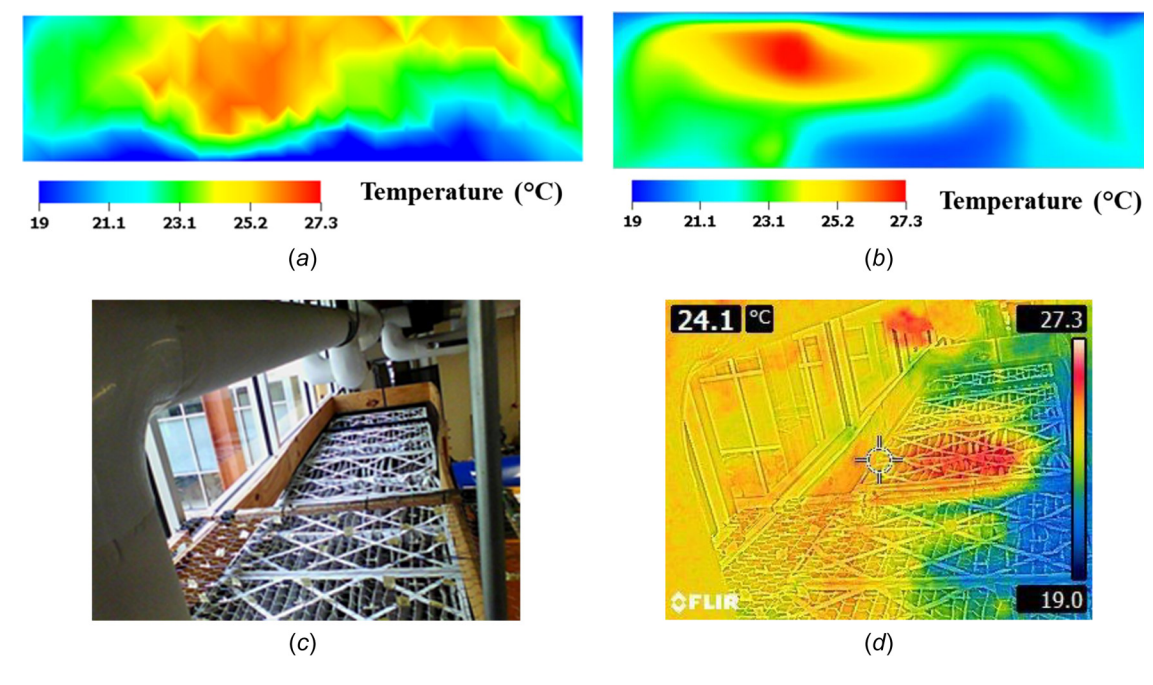


Fig. 17 Measured and simulated temperature contours at the intake of CRAH2: (a) measured air temperature, (b) simulated temperature contours, and (c) thermal IR image

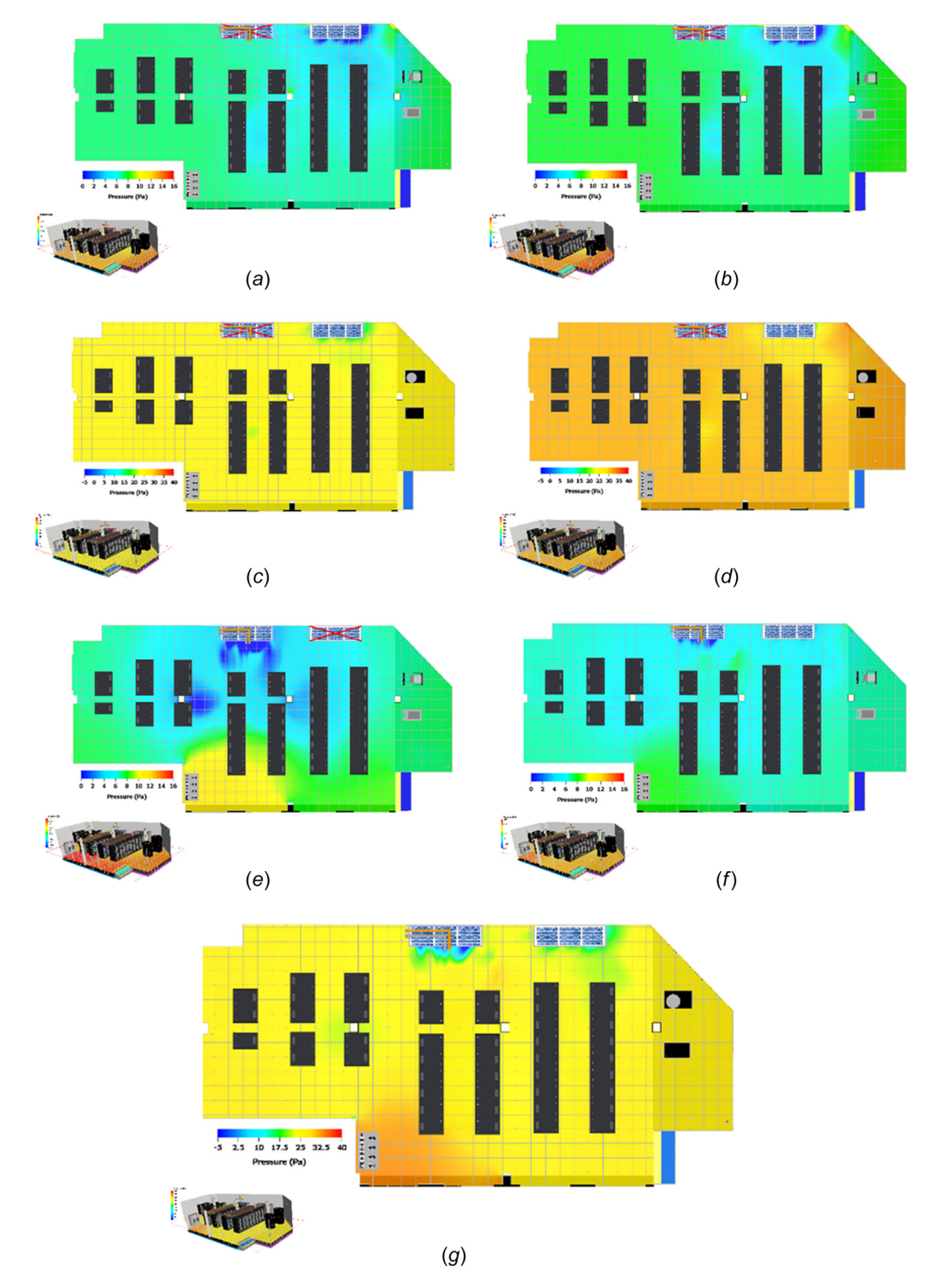


Fig. 18 (a-g) Pressure fields 1 ft below the raised floor for scenarios 1, 2, 3, 4, 5, 6, and 7, respectively

The simulation results for the airflow patterns out of the cooling units and into the floors voids demonstrate the differences in the air outlet jets for each CRAH technology. These results are presented side by side in Figs. 19(a) and 19(b), wherein the airflow patterns are colored based on velocity. Each blower technology moved the air in significantly different ways. The forward blowers directed air straight out from the unit. The backward blowers directed air biased to the blowing direction of the fans. In the case of the backward blowers, there was also a dead zone that did not receive any air, which is circled in white in Fig. 19(b). Based on airflow patterns and pressure fields, different CRAH technology

will behave differently in larger data center rooms. In the future, additional CFD models could be developed to further investigate, analyze and compare different CRAH technology deployment in hyper-scale data centers (Fig. 20).

Furthermore, to have a straightforward comparison between different CRAH technologies, two additional scenarios were modeled. In these scenarios, CRAH2 was placed at the location of CRAH1 and CRAH1 at the location of CRAH2, where only one cooling unit was on duty and the other one was powered off. Pressure fields of both cooling technologies at different locations are illustrated in Fig. 21. It can be inferred that swapping the locations

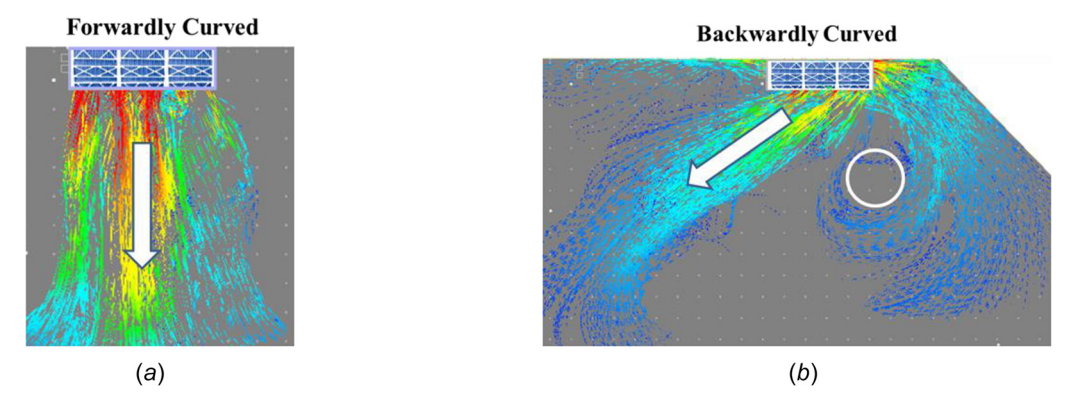


Fig. 19 Simulation airflow pattern resulting from different CRAH technology: (a) forward curved and (b) backward curved

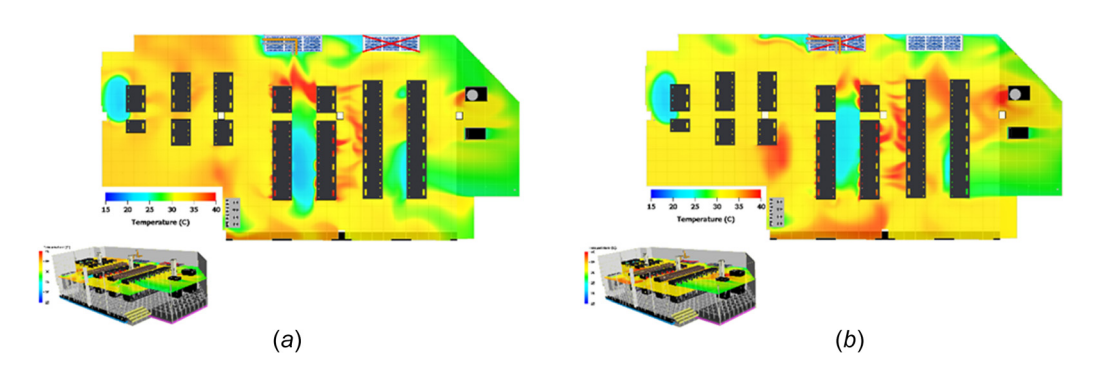


Fig. 20 Simulation temperature field 7 ft above the raised floor (horizontal plane) for scenarios 5 and 1, respectively

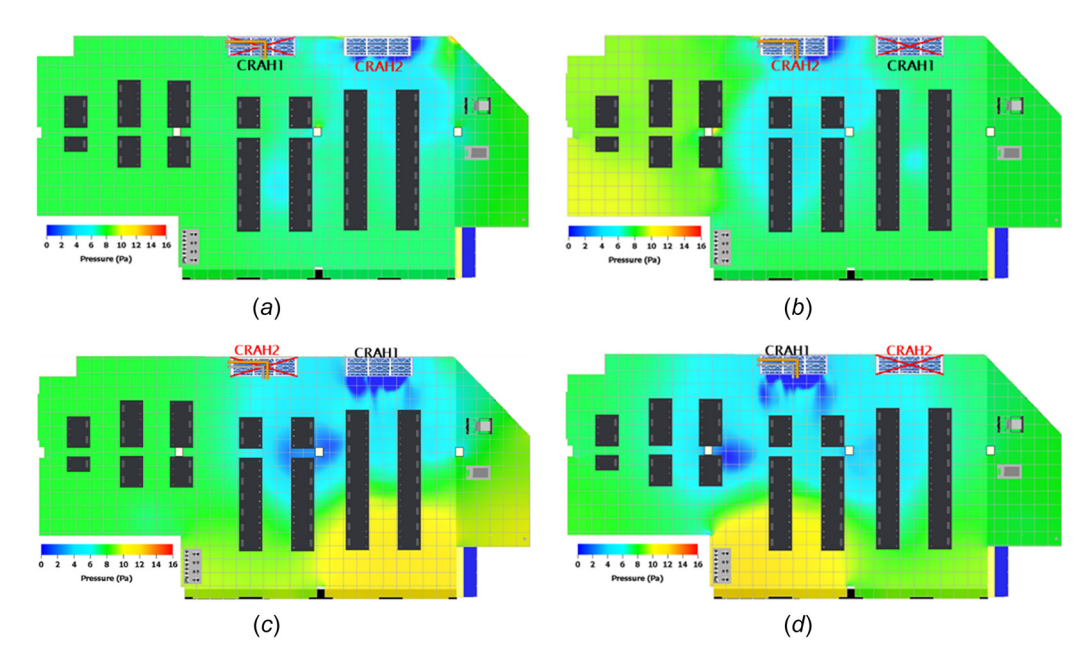


Fig. 21 Simulation pressure fields 1 foot below the raised floor: (a and b) relocated CRAH2 and (c and d) Relocated CRAH1

of CRAH2 (Figs. 21(a) and 21(b)) with CRAH1 (Figs. 21(c) and 21(d)) has an impact on the pressure distribution since it is highly dependent on the air outlet jets for each CRAH technology as demonstrated in Fig. 19.

### 4 Conclusions

The main objective of this study was to develop an overall and improved understanding of the role of backward curved blowers and to compare the resulting flow, pressure, and temperature fields with those from forwarding curved blowers. Although backward curved blowers are 30% more energy efficient, there are other important aspects of their airflow patterns that distinguish them from forwarding curved blowers. Most notably, the airflow bias toward the blowing direction can create a dead zone wherein no air is delivered to the IT.

In this study, a CFD model was validated against experimental measurements while comparing the airflow, pressure, and temperature fields of two different CRAH blower technologies when used to cool the same data center geometry and IT load. The fields induced by backward curved blowers were characterized and compared with those of forwarding curved blowers in a reference data center laboratory. It was concluded that the resulting fields were highly related to the direction of airflow from each of the examined blower technologies. Initial CFD modeling used 22% open perforated tiles to match those currently in the data center. Further simulations using tiles with higher open ratios showed that the open ratio of the perforated tiles would have no effect on the overall observations. However, the simulations did show that perforated tiles with higher open ratios would lower raised floor leakage due to the lower pressure differential between the plenum and the white space.

The major experimental and simulation results of this study can be summarized as follows:

- Containment doors constrain tile's airflow rate but do not affect the cooling unit measured intake airflow rate. Results showed a drop of 568 CFM in the total tile airflow delivery due to the introduction of an additional barrier to the air path through the aisle by containment. Thus, the floor leakage increased as well.
- The procedure used for measuring the actual airflow rate
  of cooling units is useful in practice considering the
  small (5%) margin of error compared to OEM data. However, this uncertainty may result in room pressure overestimation.
- Restraining the flow to one aisle (Aisle C here) results in a significant increase of the floor leakage, which was estimated to be 7167 and 7495 CFM for scenarios 3 and 4, respectively. The tile to CRAH airflow ratios for the flow constraint scenarios 1, 2, 3, and 4 were 85.5%, 83.9%, 61%, and 59%, respectively. The corresponding leakage ratios were 14.5%, 16%, 38.9%, and 41%, respectively.
- With respect to the different airflow patterns out from the cooling units and the spatial location of tiles with respect to the unit, the airflow delivered through perforated tiles was mostly higher for CRAH2, except for specific tiles.
- Considering the air velocity uniformity at the cooling unit intake side, the results showed that CRAH1 had a more uniform air velocity, which was related to how the air entered and exited each blower type.
- Finally, the simulation results obtained from the physicsbased CFD model showed an 8% and 16.2% mismatch from the experimental airflow and pressure measurements, respectively. The CFD model qualitatively predicted the temperature field.
- Different blowers move the air in significantly different ways. The forward blowers directed the air straight out from the unit, while the backward blower's airflow

was biased to the blowing direction of the fans. There was also a dead zone that did not get any air. Based on airflow patterns and pressure fields, different CRAH technology will behave differently in larger data center rooms.

### Acknowledgment

We would like to acknowledge Vertiv and Future Facilities Ltd. We would also like to thank the ES2 Partner Universities for their support and advice.

### **Funding Data**

 NSF IUCRC (Award No. IIP-1738793 and MRI Award No. CNS1040666; Funder ID: 10.13039/100000001).

### Nomenclature

ACU = air cooling unit

CFD = computational fluid dynamics

CRAC = compute room air conditioner

CRAH = computer room air handler

DC = data center

EC = electronically commutated

FNM = flow network model

IOM = index of mixing

OEM = original equipment manufacturer

SAT = supply air temperature

TDM = thermodynamic model

### References

- [1] Greenberg, S., Mills, E., Tschudi, B., Rumsey, P., and Myatt, B., 2006, "Best Practices for Data Centers: Lessons Learned From Benchmarking 22 Data Centers," Proceedings of the ACEEE Summer Study on Energy Efficiency in Buildings in Asilomar, ACEEE, Pacific Grove, CA, Aug. 3, pp. 76–87.
- [2] Schmidt, R., Beaty, D., and Dietrich, J., 2007, "Increasing Energy Efficiency in Data Centers," ASHRAE J., 49(12), p. 18.
- [3] Patankar, S. V., 2010, "Airflow and Cooling in a Data Center," ASME J. Heat Transfer-Trans. ASME, 132(7), p. 073001.
- [4] Hamann, H. F., Schappert, M., İyengar, M., van Kessel, T., and Claassen, A., 2008, "Methods and Techniques for Measuring and Improving Data Center Best Practices," 11th Intersociety Conference on Thermal and Thermomechanical Phenomena in Electronic Systems, IEEE, Orlando, FL, May 28–31, pp. 1146–1152.
- [5] Radmehr, A., Schmidt, R. R., Karki, K. C., and Patankar, S. V., 2005, "Distributed Leakage Flow in Raised-Floor Data Centers," ASME Paper No. IPACK2005-73273.
- [6] Iyengar, M., Schmidt, R. R., Hamann, H., and VanGilder, J., 2007, "Comparison Between Numerical and Experimental Temperature Distributions in a Small Data Center Test Cell," ASME Paper No. IPACK2007-33508.
- [7] Samadiani, E., Rambo, J., and Joshi, Y., 2010, "Numerical Modeling of Perforated Tile Flow Distribution in a Raised-Floor Data Center," ASME J. Electron. Packag., 132(2), p. 021002.
- [8] Abdelmaksoud, W. A., Khalifa, H. E., Dang, T. Q., Elhadidi, B., Schmidt, R. R., and Iyengar, M., 2010, "Experimental and Computational Study of Perforated Floor Tile in Data Centers," 12th IEEE Intersociety Conference on Thermal and Thermomechanical Phenomena in Electronic Systems, IEEE, Las Vegas, NV, June 2–5, pp. 1–10.
- [9] Garimella, S. V., Persons, T., Weibel, J. A., and Gektin, V., 2017, "Electronics Thermal Management in Information and Communications Technologies: Challenges and Future Directions," IEEE Trans. Compon., Packag. Manuf. Technol., 7(8), pp. 1191–1205.
- [10] Nada, S. A., and Said, M. A., 2017, "Comprehensive Study on the Effects of Plenum Depths on Airflow and Thermal Managements in Data Centers," Int. J. Therm. Sci., 122, pp. 302–312.
- [11] Moazamigoodarzi, H., Tsai, P. J., Pal, S., Ghosh, S., and Puri, I. K., 2019, "Influence of Cooling Architecture on Data Center Power Consumption," Energy, 183, pp. 525–535.
- [12] Lim, S. Y., and Chang, H. J., 2021, "Airflow Management Analysis to Suppress Data Center Hot Spots," Build. Environ., 197, p. 107843.
- [13] Song, P., Zhang, Z., and Zhu, Y., 2021, "Numerical and Experimental Investigation of Thermal Performance in Data Center With Different Deflectors for Cold Aisle Containment," Build. Environ., 200, p. 107961.
- [14] Manaserh, Y. M., Tradat, M. I., Gharaibeh, A. R., Sammakia, B. G., and Tipton, R., 2021, "Shifting to Energy Efficient Hybrid Cooled Data Centers Using Novel Embedded Floor Tiles Heat Exchangers," Energy Convers. Manage., 247, p. 114762.

- [15] Manaserh, Y. M., Tradat, M. I., Hoang, C. H., Sammakia, B. G., Ortega, A., Nemati, K., and Seymour, M. J., 2021, "Degradation of Fan Performance in Cooling Electronics: Experimental Investigation and Evaluating Numerical Techniques." Int. J. Heart Mass Transfer 174, p. 121291
- Techniques," Int. J. Heat Mass Transfer, 174, p. 121291.
  [16] Tradat, M. I., Khalili, S., Khatabi, M., Sammakia, B. G., Seymour, M., Tipton, R., and Alissa, H. A., 2019, "Numerical Investigation of Novel Underfloor Air-Directors Effect on Data Center Performance," 18th IEEE Intersociety Conference on Thermal and Thermomechanical Phenomena in Electronic Systems (ITherm), IEEE, Las Vegas, NV, May 28–31, pp. 886–896.
- [17] Roknaldin, F., Sahan, R. A., and Sun, X. H., 2002, May, "A Simplified CFD Model for the Radial Blower," ITherm Eighth Intersociety Conference on Thermal and Thermomechanical Phenomena in Electronic Systems (Cat. No. 02CH37258), IEEE, San Diego, CA, May 31–June 1, pp. 600–604.
- [18] Stavreva, S., and Serafimov, M., 2014, "Computational Fluid Dynamics (CFD) Analysis for Predicting the Airflow in a Data Centre," TEM J., 3(3), p. 235.
- [19] Huang, Z., Dong, K., Sun, Q., Su, L., and Liu, T., 2017, "Numerical Simulation and Comparative Analysis of Different Airflow Distributions in Data Centers," Procedia Eng., 205, pp. 2378–2385.
- [20] Yuan, X., Xu, X., Liu, J., Pan, Y., Kosonen, R., and Gao, Y., 2020, "Improvement in Airflow and Temperature Distribution With an In-Rack UFAD System at a High-Density Data Center," Build. Environ., 168, p. 106495.
- [21] Erden, H. S., Koz, M., Yildirim, M. T., and Khalifa, H. E., 2017, "Experimental Demonstration and Flow Network Model Verification of Induced CRAH Bypass for Cooling Optimization of Enclosed-Aisle Data Centers," IEEE Trans. Compon., Packag. Manuf. Technol., 7(11), pp. 1795–1803.
- [22] Wibron, E., Ljung, A. L., and Lundström, T. S., 2018, "Computational Fluid Dynamics Modeling and Validating Experiments of Airflow in a Data Center," Energies, 11(3), p. 644.
- [23] Wan, J., Gui, X., Kasahara, S., Zhang, Y., and Zhang, R., 2018, "Airflow Measurement and Management for Improving Cooling and Energy Efficiency in Raised-Floor Data Centers: A Survey," IEEE Access, 6, pp. 48867–48901.
  [24] Jin, C., Bai, X., and Yang, C., 2019, "Effects of Airflow on the Thermal Envi-
- [24] Jin, C., Bai, X., and Yang, C., 2019, "Effects of Airflow on the Thermal Environment and Energy Efficiency in Raised-Floor Data Centers: A Review," Sci. Total Environ., 695, p. 133801.

- [25] Gong, X., Zhang, Z., Gan, S., Niu, B., Yang, L., Xu, H., and Gao, M., 2020, "A Review on Evaluation Metrics of Thermal Performance in Data Centers," Build. Environ., 177, p. 106907.
- [26] Huang, J., Chen, C., Guo, G., Zhang, Z., and Li, Z., 2019, "Numerical Investigation for the Arrangement of Perforated Tile Under a Non-Uniform Heat Source Condition in a Raised-Floor Data Center," J. Phys. Conf. Ser., 1304(1), p. 012021.
- [27] Alissa, H. A., Nemati, K., Sammakia, B., Seymour, M., Schneebeli, K., and Schmidt, R., 2015, "Experimental and Numerical Characterization of a Raised Floor Data Center Using Rapid Operational Flow Curves Model," ASME Paper No. IPACK2015-48234.
- [28] Tradat, M. I., Alissa, H. A., Nemati, K., Khalili, S., Sammakia, B. G., Seymour, M. J., and Tipton, R., 2017, "Impact of Elevated Temperature on Data Center Operation Based on Internal and External IT Instrumentation," 33rd Thermal Measurement, Modeling & Management Symposium (SEMI-THERM), San Jose, CA, Mar. 13–17, pp. 108–114.
- [29] Tradat, M., Mohsenian, G., Manaserh, Y., Sammakia, B., Mendo, D., and Alissa, H. A., 2020, "Experimental Analysis of Different Measurement Techniques of Server-Rack Airflow Predictions Towards Proper DC Airflow Management," 2020 19th IEEE Intersociety Conference on Thermal and Thermomechanical Phenomena in Electronic Systems (ITherm), Orlando, FL, July 21–23, pp. 366–373.
- [30] Tradat, M. I., Manaserh, Y. "M. A.", Sammakia, B. G., Hoang, C. H., and Alissa, H. A., 2021, "An Experimental and Numerical Investigation of Novel Solution for Energy Management Enhancement in Data Centers Using Underfloor Plenum Porous Obstructions," Appl. Energy, 289, p. 116663.
- [31] Gharaibeh, A. R., Tradat, M. I., Rangarajan, S., Sammakia, B. G., and Alissa, H. A., 2021, "Multi-Objective Optimization of 3D Printed Liquid Cooled Heat Sink With Guide Vanes for Targeting Hotspots in High Heat Flux Electronics," Int. J. Heat Mass Transfer, 184, p. 122287.
  [32] Ling, Y. Z., Zhang, X. S., Zhang, K., and Jin, X., 2017, "On the Characteristics
- [32] Ling, Y. Z., Zhang, X. S., Zhang, K., and Jin, X., 2017, "On the Characteristics of Airflow Through the Perforated Tiles for Raised-Floor Data Centers," J. Build. Eng., 10, pp. 60–68.